Energy-flux characterization of conical and space-time coupled wave packets

A. Lotti,[1,2,3,*] A. Couairon,[2,3] D. Faccio,[1] and P. Di Trapani[1,3]
[1]*CNISM and Department of Physics and Mathematics, Università dell'Insubria, I-22100 Como, Italy*
[2]*Centre de Physique Théorique, CNRS, École Polytechnique, F-91128 Palaiseau, France*
[3]*VINO-Virtual Institute of Nonlinear Optics, Via Cantoni 1, I-22100 Como, Italy*
(Received 9 November 2009; published 11 February 2010)

We introduce the concept of energy density flux as a characterization tool for the propagation of ultrashort laser pulses with spatiotemporal coupling. In contrast with calculations for the Poynting vector, those for energy density flux are derived in the local frame moving at the velocity of the envelope of the wave packet under examination and do not need knowledge of the magnetic field. We show that the energy flux defined from a paraxial propagation equation follows specific geometrical connections with the phase front of the optical wave packet, which demonstrates that the knowledge of the phase fronts amounts to the measurement of the energy flux. We perform a detailed numerical study of the energy density flux in the particular case of conical waves, with special attention paid to stationary-envelope conical waves (X or O waves). A full characterization of linear conical waves is given in terms of their energy flux. We extend the definition of this concept to the case of nonlinear propagation in Kerr media with nonlinear losses.

DOI: 10.1103/PhysRevA.81.023810 PACS number(s): 42.25.Bs, 03.50.De, 42.65.Re, 42.65.Sf

I. INTRODUCTION

Femtosecond laser pulses are nowadays used for many applications that commonly require beam and pulse shaping when specific pulse temporal profiles, spectra, or beam profiles have to be maintained over a given propagation distance or available on a target. For instance, the generation of secondary radiation from the UV to the THz range can be achieved by the interaction of moderately intense pulses with a gas over long distances [1,2]. The fast ignition scheme in laser fusion needs an intense laser pulse to interact with a dense plasma over a localized area [3]. Localized energy deposition on a target is required in applications ranging from material engineering with lasers to laser surgery [4,5]. Particle-manipulation scenarios were proposed with weakly localized waves [6,7]. In these applications, wave localization and stationarity of the interaction over a given propagation distance are crucial features.

Designing wave packets with the required features necessitates excellent control of the phase and intensity distribution of the laser pulses. Several pulse- and beam-shaping techniques have been developed to spatially, temporally, or spectrally tailor specific features of Gaussian laser beams or pulses. However, complicated wave packets for which space and time are strongly coupled cannot be routinely generated in the laboratory by simply combining optical elements acting uniquely on the beam or pulse shape. An example of such pulses is the family of conical waves recently reviewed by Malaguti and Trillo [8]. These waves are of potential interest in all applications where a stationary propagation of an intense core is required over distances larger than those achievable with conventional pulses. Conical waves indeed exhibit the peculiar property of Bessel beams that the energy flux is not directed along the propagation axis as in Gaussian-like beams but arrives laterally from a cone-shaped surface [9]. This leads to the appearance of a very intense and localized interference peak which propagates without spreading over a distance $w_0/\tan\theta$ that depends on the cone angle θ and the width w_0 of the input beam. For Bessel beams, slowly decaying tails in the form of concentric rings contain a major part of the beam power and support the long propagation distance featuring conical waves. Conical waves can be viewed as the polychromatic generalization of Bessel beams in the sense that they are free of diffraction and dispersion over long distances. Several types of conical waves are well identified from the theoretical point of view [9–12]. However, their generation and even their characterization raise issues owing to their space-time coupling and weak localization.

To date, optical conical waves are known to be spontaneously generated in Kerr media by filamentation and in quadratic media [13–16]. Experimentally, conical waves have been extensively characterized by far-field measurements [17–20], but clear experimental characterization of the near-field of conical waves remains a difficult task. The three-dimensional (3D) reconstruction technique proposed in Refs. [13,21] was applied to characterize the space-time intensity distribution of a complex ultrashort pulse that underwent filamentation in water and showed the need to develop alternative methods for the retrieval of weakly decaying tails of space-time coupled wave packets [15]. Several techniques were recently proposed for measuring the space-time amplitude and phase of complex ultrashort pulses [22–24]. It was foreseen from numerical simulations that this information gives direct access to the characterization of conical waves in terms of energy flux [25,26]. Although the robustness of filaments is interpreted as resulting from an inward energy flux [27–31], an experimental characterization of the energy flux associated with filamentation dynamics has been achieved only recently [32], opening the way to a similar characterization of space-time coupled wave packets.

This article proposes the concept of density of energy flux as a tool that gives important information on pulse localization, stationarity, and dynamics. This concept is particularly important in the case of conical waves for which stationarity and localization are intimately linked to the energy flux. The energy

*antonio.lotti@uninsubria.it

flux is traditionally given by the Poynting vector. However, a diagnostic based on the Poynting vector requires knowledge of the electric and magnetic fields and the latter is not an experimentally accessible quantity. Pioneering works showed that under certain conditions the components of the Poynting vector can be expressed as functions of the transverse electric field distribution in space and time of a forward-propagating paraxial pulse [33–36]. In this article, we propose an alternative concept, namely the energy-flux density expressed in the local reference frame of the optical pulse under examination, which only requires knowledge of the intensity and phase distribution of the pulse. We comment on the link between local energy-flux density and the Poynting vector, and we illustrate the usefulness of energy-flux characterization for wave packets with space-time coupling by means of the example of linear conical waves.

Section II presents the theoretical building blocks of the article: first, the concept of energy-flux density for optical pulses with envelope satisfying a forward-propagation equation; second, the link to the Poynting vector; and third, the conical wave packets which will be characterized by their energy density flux. Section III illustrates the fundamental difference between the time-averaged energy flux, usually applied for monochromatic beams, and the local energy flux we propose for characterizing polychromatic wave packets featured by temporal localization and space-time coupling. Section IV establishes a complete characterization of linear conical waves in terms of local flux components. Section V characterizes the longitudinal component of the local energy flux. Section VI shows how the concept of energy-flux characterization extends to nonlinear unbalanced conical waves.

II. DEFINITIONS OF ENERGY DENSITY FLUX

We start by defining the notion of energy density flux. As we will see, important information regarding stationarity of a wave packet may be obtained from the energy density flux expressed in the local frame of the wave packet. We will thus define the local energy density flux in the laboratory frame as well as in the local frame moving at the group velocity of the wave packet. We consider an optical pulse of central frequency ω_0 propagating in the forward direction (negative times t) in a dispersive medium. The electric field $E(x, y, z, t)$ is decomposed into carrier and envelope as $E(x, y, z, t) = \mathcal{E}(x, y, z, t)\exp(-i\omega_0 t + ik_0 z)$, where $k_0 = \omega_0 n(\omega_0)/c$ is the modulus of the wave vector at ω_0. The linear propagation of the pulse is governed by the envelope equation

$$\frac{\partial \mathcal{E}}{\partial z} + k_0' \frac{\partial \mathcal{E}}{\partial t} = \frac{i}{2k_0}\nabla_\perp^2 \mathcal{E} - i\frac{k_0''}{2}\frac{\partial^2 \mathcal{E}}{\partial t^2}, \tag{1}$$

where $\mathcal{E}$ represents the complex amplitude of the envelope of the electric field. The derivation of Eq. (1) from Maxwell equations relies on several approximations, namely:

1. *Scalar approximation*: The pulse is assumed to be linearly polarized in a direction transverse to the propagation direction z. $\mathcal{E}$ is the scalar complex amplitude of the transverse electric field.
2. *Slowly varying envelope approximation*: The envelope shape evolves over a scale typically much larger than the wavelength. The second-order derivative $\partial^2\mathcal{E}/\partial z^2$ is negligible with respect to $k_0 \partial\mathcal{E}/\partial z$.
3. *Paraxial approximation*: $|\Delta\mathbf{k}|/k \ll 1$.
4. *Narrow bandwidth*: $|\Delta\omega|/\omega_0 \ll 1$, which justifies a second-order expansion of the dispersive terms $k(\omega)$.

The left-hand side of Eq. (1) represents the propagator, where $k_0' \equiv \partial k/\partial\omega(\omega = \omega_0)$ represents the inverse of the group velocity of the pulse, the time in the laboratory frame t represents the longitudinal coordinate, and the propagation distance z represents the evolution parameter. The first and second terms on the right-hand side of Eq. (1) represent diffraction and group velocity dispersion (GVD), respectively; $\nabla_\perp^2 = \partial^2/\partial x^2 + \partial^2/\partial y^2$ is the Laplacian in transverse coordinates, which may as well be expressed with cylindrical coordinates and $k_0'' \equiv \partial^2 k/\partial\omega^2(\omega = \omega_0)$.

A. Derivation of the energy density flux from the propagation equation

For convenience, $\mathcal{E}$ is assumed to be expressed in W/cm^2; thus, $|\mathcal{E}|^2$ represents the local intensity of the pulse. It also represents the pulse energy density in the (x, y, t) space since the magnetic part of the electromagnetic energy is negligible and the total pulse energy is given by integration of intensity over the entire space. If a volume $\mathcal{V}$ is considered in the (x, y, t) space, $\int_\mathcal{V} |\mathcal{E}|^2 dxdydt$ represents the total energy carried by the pulse in region $\mathcal{V}$ and satisfies a conservation equation obtained by multiplying Eq. (1) by $\mathcal{E}^*$, summing the result with its complex conjugate and performing the volume integration. Locally, the energy-conservation equation takes a form analogous to the divergence theorem,

$$\frac{\partial |\mathcal{E}|^2}{\partial z} = -\widetilde{\mathrm{div}}\mathbf{J}, \tag{2}$$

where the divergence operator is defined in the (x, y, t) space as $\widetilde{\mathrm{div}}\mathbf{F} = \nabla_\perp \cdot \mathbf{F}_\perp + \partial F_t/\partial t$. This allows for an identification of the flux of energy density $\mathbf{J}$ through the surface $\mathcal{S}$ enclosing volume $\mathcal{V}$:

$$\mathbf{J}_\perp = \frac{1}{2ik_0}[\mathcal{E}^*\nabla_\perp\mathcal{E} - \mathcal{E}\nabla_\perp\mathcal{E}^*] \tag{3}$$

$$J_t = k_0'|\mathcal{E}|^2 - \frac{k_0''}{2i}\left[\mathcal{E}^*\frac{\partial\mathcal{E}}{\partial t} - \mathcal{E}\frac{\partial\mathcal{E}^*}{\partial t}\right]. \tag{4}$$

The longitudinal component defined by Eq. (4) includes two contributions: the first term is associated with the propagation of the pulse at velocity $V_G = k_0'^{-1}$, whereas the second contribution is intrinsic to the propagation medium and associated with dispersion. The longitudinal energy density flux in the local frame of the pulse, associated with the local time $\tau = t - k_0' z$, thus reads

$$J_\tau = -\frac{k_0''}{2i}\left[\mathcal{E}^*\frac{\partial\mathcal{E}}{\partial\tau} - \mathcal{E}\frac{\partial\mathcal{E}^*}{\partial\tau}\right], \tag{5}$$

whereas the transverse component is unchanged. In this frame, the energy density flux entails information on the relative redistribution of energy in the (x, y, τ) space during propagation. If the complex envelope is written in terms of amplitude and phase $\mathcal{E} = |\mathcal{E}|\exp(i\phi)$, each of the energy-flux components is shown to be proportional to the intensity and to

the phase gradient along the corresponding direction:

$$\mathbf{J} = \frac{1}{k_0}|\mathcal{E}|^2 \left(\nabla_\perp \phi, -k_0 k_0'' \frac{\partial \phi}{\partial \tau} \right). \tag{6}$$

Therefore, if it is possible to have access experimentally to the intensity and phase distributions of an optical pulse, as recently shown, for example, in Refs. [24,32,37–39], the longitudinal and transverse components of the energy density flux vector $\mathbf{J}$ are fully determined [32]. As will be seen in Sec. II C, this result still holds for a wave packet moving at velocity V different from $k_0'^{-1}$, provided corrections are made to account for the moving frame. Equation (6) also shows that the flux is proportional to the intensity distribution, indicating that features of a space-time coupled wave packet may be undetectable when an (x, y, t) intensity distribution is measured by the 3D mapping technique but visible in the flux distribution. For instance, the weighting effect introduced by the phase gradient may enhance the contrast in the weak tails [15,32].

B. Link to the Poynting vector

In classical electromagnetism, the evolution of the energy density defined as $w = \mathrm{Re}\{\mathbf{E}\cdot\mathbf{D}^* + \mathbf{B}\cdot\mathbf{H}^*\}/2$ (where $\mathbf{D}$, $\mathbf{B}$, and $\mathbf{H}$ denote the electric displacement field, the magnetic induction, and the magnetic field, respectively) is governed by the conservation equation

$$\frac{\partial w}{\partial t} = -\mathrm{div}\mathbf{S}, \tag{7}$$

where $\mathbf{S} \equiv \mathrm{Re}\{\mathbf{E}\times\mathbf{H}^*\}/2$ denotes the Poynting vector and the divergence operator follows here from the standard definition: $\mathrm{div}\mathbf{F} = \nabla_\perp \cdot \mathbf{F}_\perp + \partial F_z/\partial z$. Several works have shown that the transverse component of the Poynting vector corresponds exactly to the expression given by Eq. (3); thus, $\mathbf{S}_\perp = \mathbf{J}_\perp$ [33–36,40] (see also Appendix A) . The longitudinal component S_z, however, must be interpreted differently from the local longitudinal energy flux J_τ. The density of electromagnetic energy indeed includes an electric and a magnetic contribution and the Poynting vector represents the energy density flux for both contributions in the laboratory frame. In contrast, the energy density flux $\mathbf{J}$ accounts for the electric part only. Appendix A shows that the continuity equations [Eqs. (7) and (2)], and therefore Eqs. (3) and (4), can be transformed into each other. However, the information on the dispersive properties of the medium that is contained in the longitudinal component J_τ of the energy density flux is not present in the longitudinal component of the Poynting vector S_z but in the time derivative of the electromagnetic energy. Both quantities are linked by the following expression, derived in Appendix A:

$$\frac{\partial J_t}{\partial t} = \frac{\partial}{\partial z}(S_z - |\mathcal{E}_x|^2) + \frac{\partial}{\partial t}(w_e + w_m). \tag{8}$$

We note that although there is a clear link between $\mathbf{J}$ and $\mathbf{S}$, experimental evaluation of energy density flux requires the use of $\mathbf{J}$ as defined in this work since it relies on the knowledge of the electric field alone. On the other hand, theoretical studies in which one has direct access to $\mathbf{E}$ and $\mathbf{H}$ permit the use of the energy density flux based on the Poynting vector $\mathbf{S}$ [41].

Finally we underline that there is no obvious route for deriving J_τ directly from $\mathbf{S}$ without further approximation. The Poynting vector indeed describes the energy flux when Maxwell equations describe the propagation of the pulse. Rather, we have shown that the transverse component $\mathbf{J}_\perp$ and the longitudinal component J_τ are derived from the envelope-propagation equation and that $\mathbf{J}_\perp$ coincides with $\mathbf{S}_\perp$. We show in Appendix B that for nondispersive media, a generalization of the longitudinal flux component J_τ may be expressed as $w - S_z/c$, whereas the longitudinal component of the Poynting vector S_z represents the energy density in the (x, y, t) space. This link to the Poynting vector is compatible with the expressions for the flux found under the envelope approximation. We expect that further generalization is possible in dispersive media; however, both w and S_z require the knowledge or measurement of the magnetic field, whereas within the approximations considered in this article $\mathbf{J}$ can be obtained from the knowledge of the intensity and phase of the envelope of the electric field only.

C. Linear conical waves, Bessel X pulse, and pulsed Bessel beams

We consider scalar wave packets (WPs) propagating in a dispersive medium characterized by a refractive index $n(\omega)$, thus satisfying the wave equation expressed in the Fourier domain,

$$\left[\frac{\partial^2}{\partial z^2} + \Delta_\perp + k^2(\omega) \right] E(r, \omega, z) = 0, \tag{9}$$

where $k(\omega) \equiv \omega n(\omega)/c$. WPs with central frequency ω_0 are assumed to be described by a complex envelope $\Psi(r, \tau = t - z/V, z)$ propagating in the forward direction at velocity V, possibly different from $V_G = 1/k_0'$, and a carrier wave $\exp(i\beta z - i\omega_0 t)$, where the carrier wave number β may also differ from k_0 and τ denotes the local time in the envelope frame. In particular, we may define the velocity at which the energy of the pulse propagates as $V_E = V_G \cos\theta_0$, where θ_0 is a characteristic angle of the propagating WP described below. In this work the difference between V_G and V_E from a practical point of view is always negligible; we therefore choose to name *superluminal* a velocity V greater than the Gaussian velocity V_G and *subluminal* a velocity V lower than V_G. The propagation equation governing the envelope spectrum reads

$$\left[\frac{\partial^2}{\partial z^2} + 2i\left(\beta + \frac{\Omega}{V}\right)\frac{\partial}{\partial z} + \Delta_\perp + k_\perp^2(\Omega) \right] \hat{\Psi}(r, \Omega, z) = 0, \tag{10}$$

where

$$k_\perp^2(\Omega) \equiv k^2(\omega) - (\beta + \Omega/V)^2, \tag{11}$$

and $\Omega \equiv \omega - \omega_0$ denotes the frequency departure from the carrier frequency. The general solution to Eq. (10) propagating in the forward direction with revolution symmetry reads

$$\Psi(r, \tau, z) = \frac{1}{2\pi}\int_{-\infty}^{+\infty} d\Omega \int_0^{+\infty} dK\, K \hat{A}(K, \Omega) J_0(Kr) \times \exp(i\kappa z - i\Omega\tau), \tag{12}$$

where K is the transverse component of the wave vector, $\hat{A}(K, \Omega)$ denotes an arbitrary function which represents the complex angular spectrum of the WP at $z = 0$, and the

longitudinal wave number associated with the envelope reads

$$\kappa = \left(\beta + \frac{\Omega}{V}\right)\left[\sqrt{1 + \frac{k_\perp^2(\Omega) - K^2}{(\beta + \Omega/V)^2}} - 1\right] = \sqrt{k^2(\omega) - K^2} - \left(\beta + \frac{\Omega}{V}\right). \quad (13)$$

Conical wave packets (CWPs) correspond to specific choices of the angular spectrum $\hat{A}(K, \Omega) = \hat{f}(\Omega)\delta(K - k(\omega)\sin[\theta(\Omega)])$, where $\hat{f}(\Omega)$ is a weight function for which the WP may be viewed as a superposition of plane waves with frequency-dependent wave numbers K distributed over cones of angle $\theta(\Omega)$ with respect to the propagation direction z.

The pulsed Bessel beam (PBB) and the Bessel X pulse (BXP) are particular cases of conical waves obtained from Eqs. (12) and (13) for which the plane-wave constituents present a constant transverse component of the k vector (PBB, $\theta(\Omega) = \arcsin[K_0/k(\omega)]$) [42] or a constant propagation angle θ_0 for each frequency (BXP, $K(\Omega) = k(\omega)\sin\theta_0$) [11]. The PBB is similar to a Bessel beam generated by means of a circular diffraction grating and may be regarded as the product of a Bessel beam and a Gaussian pulse. The BXP can be generated by sending a Gaussian beam through an axicon and exhibits a two-winged (X-shaped) structure resulting from the superposition of an inward and an outward beam [37,42,43]. Ideally, the PBB and the BXP have infinite energy due to their weakly decaying tails, but in practice both are produced with finite energy beams sent through finite apertures and thus exhibit a central intensity peak that extends over a propagation region called the Bessel zone (which depends on the spatial apodization of the profile).

Conical waves with a stationary envelope in their reference frame constitute an important subclass of CWP for which the envelope does not depend on z. This condition is satisfied when the longitudinal wave number varies linearly with frequency, which is obtained by choosing the angular spectrum $\hat{A}(K, \Omega) = \hat{f}(\Omega)\delta(K - k_\perp(\Omega))$ and $k_\perp(\Omega)$ is defined by Eq. (11). The envelope then reads

$$\Psi(r, \tau) = \int_{k_\perp(\Omega)\text{real}} \hat{f}(\Omega) J_0(k_\perp(\Omega) r) \exp(-i\Omega\tau) d\Omega, \quad (14)$$

where integration is performed over frequencies for which $k_\perp(\Omega)$ is real.

It is particularly instructive to assume that a small Ω expansion of the dispersion relation up to second order is sufficient to describe the dispersive properties of the medium; thus, $k(\omega) \simeq k_0 + k_0'\Omega + k_0''\Omega^2/2$ and

$$k_\perp^2(\Omega) = \alpha_2\Omega^2 + 2\alpha_1\Omega + \alpha_0, \quad (15)$$

where $\alpha_2 = k_0 k_0'' + k_0'^2 - 1/V^2$, $\alpha_1 \equiv k_0 k_0' - \beta/V$, and $\alpha_0 = k_0^2 - \beta^2$.

In this case, the stationary CWPs have been obtained by Porras and Di Trapani [44] and were recently studied in a nonparaxial framework by Malaguti and Trillo [8]. A comprehensive analysis of angular dispersion curves of stationary CWPs in a linear dispersive medium is given in Ref. [45]. In the following treatment we will refer to the notation of Ref. [8]. Stationary CWPs are characterized by two parameters: the angular aperture θ_0 of the beam

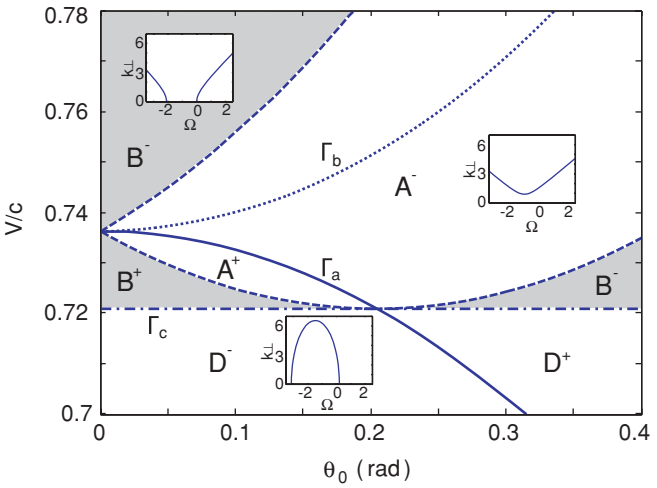

FIG. 1. (Color online) Parameter space (θ_0, V) for stationary CWP in water and a central wavelength of 527 nm. The different sectors labeled A, B, and D are bounded by the dashed curves where $\alpha_1^2 = \alpha_2\alpha_0$ and $\alpha_2 = 0$ (line Γ_c), on which the shape of the angular spectrum $k_\perp(\Omega)$ [Eq. (15)] changes. A, X waves (hyperbolic) with angle gap; B, X waves (hyperbolic) with frequency gap; D, O waves (elliptic). The $\pm$ labels indicate that the central frequency of the $k_\perp(\Omega)$ curve is upshifted (+) or downshifted (−) with respect to ω_0. The curves Γ_a ($V = V_G\cos\theta_0$) and Γ_b ($V = V_G/\cos\theta_0$) determine loci around which stationary CWPs with sufficiently narrow bandwidth share the features of PBBs or BXPs, respectively. The insets show the qualitative shape of the dispersion curve [Eq. (15)] for B^-, A^-, and D^- ($k_\perp$ in μm^{-1}, Ω in rad/fs).

at the carrier frequency which is linked to the longitudinal wave number $\beta = k_0\cos\theta_0$ and the velocity V of the CWP. Following Malaguti and Trillo, Fig. 1 shows the different types of stationary conical waves in the plane (θ_0, V), which we will use to illustrate the use of energy flux as a tool for characterizing stationary CWPs. This classification is based on a second-order approximation of chromatic dispersion, but spectral features and the characterization of the energy flux remain qualitatively similar even if the full dispersion curve is retained, as in all numerical results in this article. A single exception exists when the spectrum of the WP is centered around a zero of the GVD, which will not be treated in this article. The line Γ_c is defined by $\alpha_2 = 0$. The region above line Γ_c corresponds to X-wave solutions ($\alpha_2 > 0$). In particular, regions $A^\pm$ ($\alpha_1^2 - \alpha_2\alpha_0 < 0$ or $k_0'\cos\theta_0 - \sqrt{k_0 k_0''}\sin\theta_0 \leqslant V^{-1} \leqslant k_0'\cos\theta_0 + \sqrt{k_0 k_0''}\sin\theta_0$) correspond to hyperbolic solutions of Eq. (15) with a wave number (angle) gap, while regions $B^\pm$ ($\alpha_1^2 - \alpha_2\alpha_0 > 0$ or shaded areas in Fig. 1) correspond to hyperbolic solutions with a frequency (wavelength) gap. The region below line Γ_c corresponds to O-wave-like solutions ($\alpha_2 < 0$), which present elliptic $k_\perp(\Omega)$ profiles and are analogous to the solutions found in the case of anomalous GVD [42,44,46].

In general the PPB and the BXP are not stationary solutions in the strict sense. However, it is possible to find some limit case in which stationary CWPs may be considered as belonging to the family of PBB or BXP within this second-order expansion. From Eq. (15), it can be seen that a constant $k_\perp$ (thus a PBB profile) is obtained for $\alpha_1 = 0$ and

$\alpha_2 = 0$, which results in a single couple of velocity and angular aperture $V = V_G \cos\theta_0$ and $\tan^2\theta_0 = k_0 k_0''/k_0'^2$, respectively, corresponding to the intersection of lines Γ_a and Γ_c in Fig. 1. However, the weight function $\hat{f}(\Omega)$ may be sufficiently narrow to neglect $\alpha_2\Omega^2$ in Eq. (15), while the condition $\alpha_1 = 0$ just gives the velocity featuring a PBB so that the whole curve Γ_a ($V = V_G \cos\theta_0$) characterizes PBB-like solutions. Similarly, the angular aperture at a given frequency of the stationary CWP presented in Fig. 1 is given by $\cos\theta(\Omega) = (\beta + \Omega/V)/(k_0 + k_0'\Omega + k_0''\Omega^2/2)$. This shows that stationary conical waves with strictly constant cone angles (BXP) are never obtained in condensed media. However, if the bandwidth of the weight function in Eq. (14) allows us to neglect $k_0''\Omega^2$ in front of $k_0 + k_0'\Omega$, we obtain stationary CWPs with almost constant cone angle θ_0 for the velocity $V \sim V_G \cos\theta_0$ featuring solutions of the BXP type (line Γ_b in Fig. 1).

Finally, within the framework of the second-order expansion of $k(\omega)$ and the slowly varying envelope approximation [$\frac{\partial^2}{\partial z^2} \ll \beta\frac{\partial}{\partial z}$ in Eq. (10)], the propagation equation for the envelope $\Psi(r, \tau, z)$ can be put in the form of Eq. (1):

$$2i\beta\frac{\partial\Psi}{\partial z} + \Delta_\perp\Psi - \alpha_2\frac{\partial^2\Psi}{\partial\tau^2} + 2i\alpha_1\frac{\partial\Psi}{\partial\tau} + \alpha_0\Psi = 0. \quad (16)$$

Therefore, the associated energy-flux components are expressed as

$$\mathbf{J}_\perp = \frac{1}{2i\beta}\left[\Psi^*\nabla_\perp\Psi - \Psi\nabla_\perp\Psi^*\right], \quad (17)$$

$$J_\tau = -\frac{\alpha_2}{2i\beta}\left[\Psi^*\frac{\partial\Psi}{\partial\tau} - \Psi\frac{\partial\Psi^*}{\partial\tau}\right] + \frac{\alpha_1}{\beta}|\Psi|^2. \quad (18)$$

III. MONOCHROMATIC VS POLYCHROMATIC ENERGY DENSITY FLUX

A. Time-integrated flux

The energy density flux given in Eqs. (3) and (5) is particularly well suited to characterize polychromatic wave packets such as those presented in Sec. II C, which exhibit space-time couplings and/or angular dispersion. In most cases studied in the literature, optical wave packets are supposed to be describable in terms of separated variables with uncoupled beam and pulse dynamics. This is the case for the Gaussian pulse (GP) obtained by focusing a laser beam with a lens with focal length f in a dispersive medium. The linear propagation of a GP is well known and may be described in terms of the beam and pulse parameters solely depending on the propagation distance, with the origin ($z = 0$) at the focus of the lens [47]:

$$\mathcal{E}(r, t, z) = \mathcal{E}_0\frac{w_0 T_0^{1/2}}{w(z)T^{1/2}(z)}\exp\left[-\frac{r^2}{w(z)^2} - \frac{\tau^2}{T(z)^2}\right] \times \exp\left[ik_0\frac{r^2}{2F(z)} - i\zeta(z) - i\frac{\tau^2}{2k_0'' L(z)}\right], \quad (19)$$

where the beam waist, beam curvature, Gouy shift, pulse duration, and pulse chirp are given, respectively, by

$$w(z) = w_0\left(1 + z^2/z_R^2\right)^{1/2},$$
$$F(z) = z\left(1 + z_R^2/z^2\right),$$
$$\zeta(z) = \arctan(z/z_R),$$
$$T(z) = T_p\left[1 + (z+d)^2/z_{\mathrm{GVD}}^2\right]^{1/2},$$
$$L(z) = (z+d)\left[1 + z_{\mathrm{GVD}}^2/(z+d)^2\right].$$

Here, a flat temporal phase is assumed at the beginning of the propagation $z = -d$ defined by $f = -d - z_R^2/d$. The quantity $z_R = k_0 w_0^2/2$ denotes the Rayleigh length and $z_{\mathrm{GVD}} = T_p^2/2k_0''$ the dispersion length. The pulse duration at the focus T_0 is linked to the initial pulse duration T_p by the relation $T_0 = T_p(1 + d^2/z_{\mathrm{GVD}}^2)^{1/2}$. From Eq. (19), it is readily seen that variables are separated: the temporal (or longitudinal) and the transverse dynamics remain completely uncoupled.

When experimental characterization deals with the spatial dynamics, the temporal dynamics is assumed to be frozen and the pulse is considered as quasimonochromatic. In this case, a characterization in terms of energy flux amounts to considering the transverse component of the flux only. As we have seen, it is proportional to the intensity of the wave packet and to the transverse gradient of the wave-packet phase. If the latter quantity is assumed not to depend on time, the time-integrated flux can be approximated as

$$\mathcal{J}_\perp(r, z) = \int\mathbf{J}_\perp(r, \tau, z)d\tau \equiv \frac{1}{k_0}\int|\mathcal{E}(r, \tau, z)|^2\nabla_\perp\phi(r, z)d\tau \sim \frac{1}{k_0}\mathcal{F}(r, z)\nabla_\perp\phi(r, z), \quad (20)$$

where $\mathcal{F}(r, z) \equiv \int|\mathcal{E}(r, \tau, z)|^2 d\tau$ denotes the fluence of the beam which is the experimentally accessible quantity.

As we shall show, a fundamental difference exists between the various notions of energy flux; namely, $\mathcal{J}_\perp(r, z)$ gives us information about the fluence in the monochromatic case. In contrast, the transverse energy flux $\mathbf{J}_\perp(r, \tau, z)$ for each propagation distance gives information on the spatial and temporal reorganization of energy within the wave packet, which applies for polychromatic cases as well. The difference will be shown by considering simple situations—a GP, an apodized PBB, and an apodized BXP coming from an ideal axicon—which exhibit different space-time coupling and cannot be distinguished from their characterization by means of $\mathcal{J}_\perp(r, z)$, whereas the energy-flux characterization with $\mathbf{J}_\perp(r, \tau, z)$ clearly shows their distinct features.

B. Energy flux in the monochromatic case

For the GP, the components of $\mathbf{J}$ can be calculated directly from Eq. (19):

$$J_r = |\mathcal{E}(r, \tau, z)|^2\frac{r}{F(z)} \quad (21)$$

$$J_\tau = |\mathcal{E}(r, \tau, z)|^2\frac{\tau}{L(z)}. \quad (22)$$

From this expression, it is readily seen that $\mathcal{J}_\perp = \int J_r d\tau = \mathcal{F}(r, z)\frac{r}{F(z)}$. Thus, a GP is associated with an inward flux before the focus of the lens [$F(z) < 0$] and an outward flux after the focus.

For the PBB and the BXP, the flux is calculated numerically by considering propagation through water for WP with central frequency at $\lambda_0 = 800$ nm. The GP parameters are $w_0 = 0.03$ cm, $T_p = 80$ fs, and $f = 4$ cm. We chose PBB and

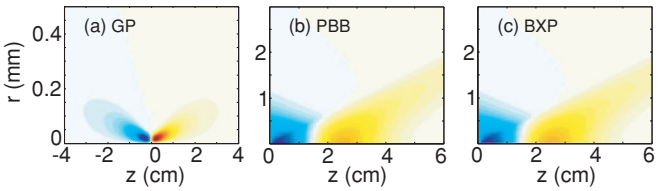

FIG. 2. (Color online) Time-integrated transverse flux profiles vs propagation distance for (a) a focused Gaussian pulse, (b) a pulsed Bessel beam, and (c) a Bessel X pulse. Red (blue) indicates outward (inward) flux with respect to the propagation axis.

BXP with the same propagation angle $\theta_0 = 2^o$ at the central wavelength $\lambda_0 = 800$ nm, temporal duration $T_p = 80$ fs, and Gaussian apodization with $w_0 = 0.1$ cm to mimic a real situation with finite energy.

Figure 2 shows the time-integrated transverse flux $\mathcal{J}_\perp(r, z)$ as a function of the propagation distance z (evolution parameter) and radial coordinate for the three cases under examination. The focused Gaussian case [Fig. 2(a)] presents inward-directed (negative) flux before the beam waist position at $z = 0$ and outward-directed (positive) beyond the focus, due to linear diffraction. As can be seen in Figs. 2(b) and 2(c), the cases of the PBB and the BXP cannot be distinguished by their characterization in terms of time-integrated flux. Both exhibit an integrated flux qualitatively similar to that of a GP, with an initial inward flux, followed by a region (corresponding approximatively to the center of the Bessel zone) in which the flux vanishes, and finally an outward flux. This behavior is strictly connected to the fact that the beams are spatially apodized, as will be discussed later. For longer propagation distances, the flux becomes ring-shaped (in the x-y plane), which corresponds to the far field of a PBB or a BXP.

C. Energy flux in the polychromatic case

The representation at fixed z of J_r in the (r, τ) domain allows us to discriminate between the three cases. Figure 3 shows the change in the transverse flux distribution for the GP, PBB, and BXP as a function of the propagation distance.

Before the focus of the GP or at the very input of the Bessel zone [Figs. 3(a)–3(c)], the GP transverse flux does not present any spatiotemporal feature, indicating that the pulse as a whole is focusing, since $J_r < 0$. The PBB and the BXP present an inward energy flux, featured by the intensity distribution of the wave packet itself. Figures 3(d)–3(f) show the three cases around the beam waist or the center of the Bessel zone. The GP transverse flux [Fig. 3(d)] is considerably smaller with respect to the previous case since the WP is approaching the beam waist.

The BXP flux [Fig. 3(f)] presents two wings: one in the leading part of the pulse with inward-directed flux and one in the trailing part with outward-directed flux. This behavior may be simply understood by means of Fig. 4(a) as a result of the conical nature of this wave packet. The PBB can be regarded as a degenerate BXP, in which propagation angle and pulse tilt angle are equal, so that the inward-flux and outward-flux wings spatially overlap. Figures 3(g)–3(i) show the flux characterizing the GP, PBB, and BXP at a greater propagation distance. The energy flux is directed outward for all wave packets and exhibits features of the intensity distribution in the far-field region, which corresponds to a diverging Gaussian beam for the GP and a diverging ring for the PBB and the BXP.

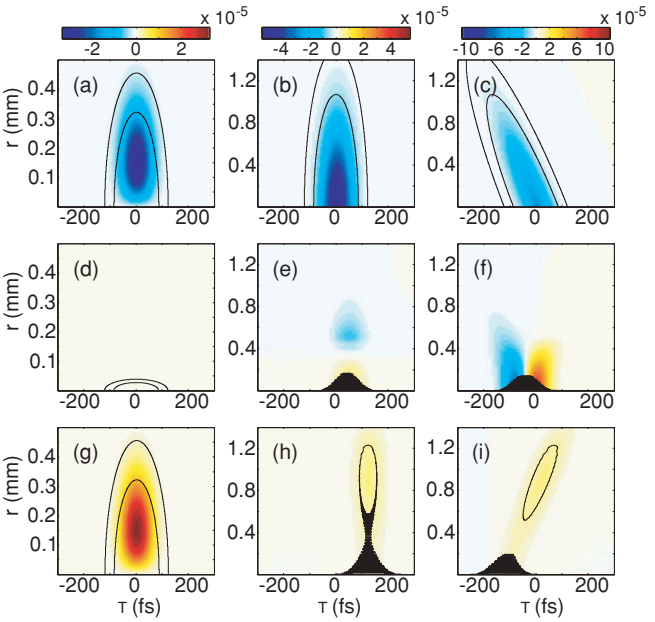

FIG. 3. (Color online) Transverse flux J_r for different wave packets at different propagation distances. Panels (a), (d), and (g) refer to the GP 4 cm before the beam waist, near the beam waist, and 4 cm after that point, respectively. Panels (b), (e), and (h) refer to a PBB obtained by multiplying a Gaussian profile by a radially dependent phase at the beginning of propagation, near the center of the Bessel zone, and toward the end of this zone, respectively. Panels (c), (f), and (i) refer to the same situation as panels (b), (e), and (h) for the BXP wave-packet profile. The color scale of J_r is in arbitrary units since the intensities were normalized to the maximum value reached during propagation. The black contour plots show the intensity over two decades.

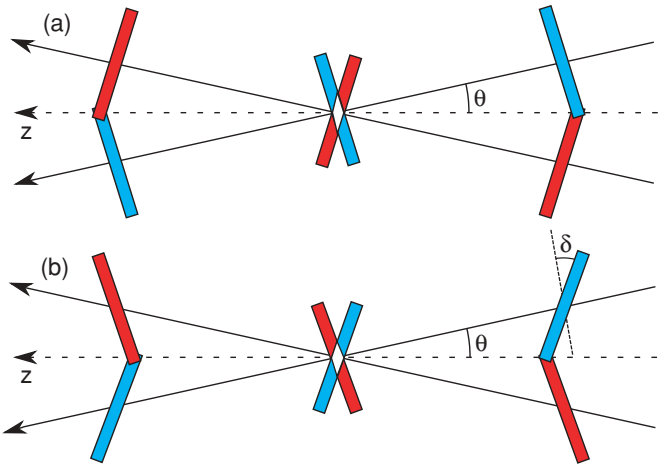

FIG. 4. (Color online) Simple representation of the propagation of the expected transverse flux for the propagation of (a) a BXP and (b) a rotationally symmetric tilted pulse. The red (blue) color corresponds to flux directed upward (downward) with respect to the vertical axis.

IV. STATIONARY ENVELOPE WAVES

A. Normal GVD case: X waves

As previously stated, stationary CWPs may be described by means of Eq. (14). Malaguti and Trillo have derived closed-form analytical solutions for stationary CWPs with specific spectral weight functions $f(\Omega)$ [8]. From these solutions and Eqs. (17) and (18), we evaluated the energy flux characterizing CWPs: All the solutions of Ref. [8] with velocity equal to the energy velocity $V_E = V_G \cos\theta_0$ and corresponding to symmetrically distributed spectral weight turn out to have both transverse and longitudinal flux components equal to 0. The case of an asymmetric spectral weight leads to analytical solutions featuring a single branch of an X wave with frequency gap in region B of Fig. 1.

In this section we will show the flux of stationary CWPs with asymmetric spectral weight, evaluated by means of Eq. (14). It is important to emphasize that we used a full dispersion relation $k(\omega)$, extrapolated from the data of [48], in the definition of these WPs [Eq. (11)]: The expression for the flux has been derived in the second-order approximation and gives the main contribution. Higher-order terms become more important in a spectral region corresponding to zero GVD.

Figure 5 shows the transverse flux J_r for an X wave corresponding to region B of Fig. 1, with central wavelength $\lambda_0 = 527$ nm, reference angle $\theta_0 = 0$ rad, Gaussian spectral weight ($T_p = 80$ fs), and Gaussian spatial apodization ($w_0 = 0.5$ mm), propagating in water when the velocity of the pulse peak is subluminal [Fig. 5(a), $V = 0.9995 V_G$] or superluminal [Fig. 5(b), $V = 1.0005 V_G$] with respect to the Gaussian group velocity $V_G = 1/k_0' = 220720072$ m/s. The flux profile is similar to that of the BXP case.

It may be noticed that the inward-directed flux wing appears in the leading part of the pulse or the trailing one according to the superluminal or subluminal propagation of the envelope peak. This behavior is not in contradiction with the fact that the overall pulse is moving in the forward direction and it may be simply understood by considering that the propagation of the central peak is the result of the cylindrically symmetric superposition of tilted pulses, as already pointed out in [42] and schematically represented in Fig. 4(b).

Spatial apodization limits the propagation range in which the wave packet is effectively stationary: the behavior is

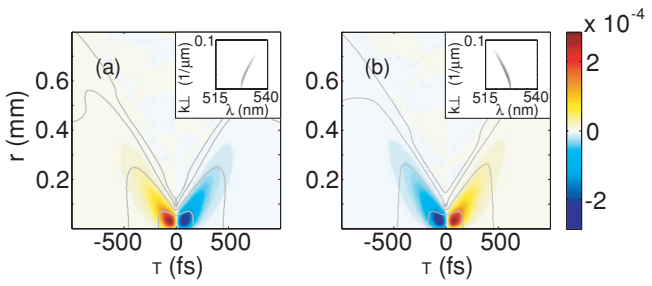

FIG. 5. (Color online) Transverse flux J_r for stationary CWP in the X-wave case for different propagation velocities of the envelope peak. (a) $V = 0.9995 V_G$; (b) $V = 1.0005 V_G$. The gray contour plots show the intensity over four decades. The insets show the corresponding spectral $\lambda, k_\perp$ features. Color scale in arbitrary units.

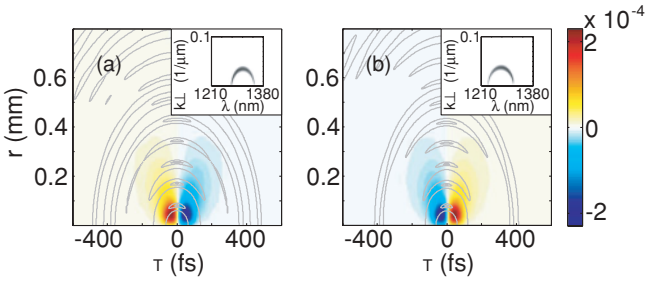

FIG. 6. (Color online) Transverse flux J_r for stationary CWP of the O-wave type for different propagation velocities of the envelope peak. (a) $V = 0.9995 V_G$; (b) $V = 1.0005 V_G$. The gray contour plots show the intensity over four decades. The insets show the corresponding spectral $\lambda, k_\perp$ features. Color scale in arbitrary units.

qualitatively similar to the BXP case. After propagation toward the end of the Bessel zone, a dominant wing carrying an outward-directed flux is obtained in the trailing or leading part of the pulse depending on the peak velocity (superluminal in the first case and subluminal in the second case).

B. Anomalous GVD case: O waves

Stationary CWPs in media with anomalous dispersion typically feature elliptical spectral $k_\perp(\Omega)$ profiles called O waves [44,49]. Similar stationary CWPs are also obtained in the case of normal dispersion [8] in region D in Fig. 1; however, these profiles are either highly nonparaxial or are almost identical to a single-branch X-wave profile if we remain in a paraxial frame.

In this section we will study the O-wave case within the paraxial approximation by considering the propagation in a medium with anomalous GVD ($k_0'' < 0$). As in the previous section, we will consider the full dispersion relation in the definition of the wave packet and an asymmetrical spectral weight.

Figure 6 shows the transverse flux J_r for this WP propagating in water at central wavelength $\lambda_0 = 1300$ nm and corresponding angle $\theta_0 = 0.005$ rad, Gaussian spectral weight ($T_p = 40$ fs), Gaussian spatial apodization ($w_0 = 0.6$ mm), peak velocity [Fig. 6(a) $V = 0.9995\ V_G$ and Fig. 6(b) $V = 1.0005\ V_G$] greater and lower than $V_G = 222930323$ m/s, respectively. Although the near-field profile of the wave packet under examination is definitely different from that of the X-wave case, it still exhibits an almost identical flux profile and we are still able to predict super- or subluminal velocity by looking at the position of the inward-directed energy wing.

V. LONGITUDINAL COMPONENT AND ENERGY STREAM

Up to now, we considered only the transverse component of the energy flux **J**, which coincides with the transverse component of the Poynting vector and does not depend on the velocity of the wave packet under examination. In this section, we show that the longitudinal component of the energy flux also constitutes an important source of information that we exploit in two different forms: First, we consider the

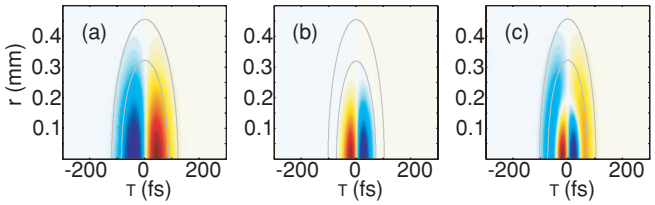

FIG. 7. (Color online) Longitudinal flux J_τ for a GP propagating in different regimes. (a) Linear propagation with normal GVD. (b) Nonlinear propagation (high intensity) with anomalous GVD ($\lambda_0 = 1300$ nm in water). (c) Nonlinear propagation with anomalous GVD at lower intensity with respect to case (b). The color scale of J_τ indicates flux toward positive (negative) τ values in red (blue). The gray contour plots show intensity contours over two decades.

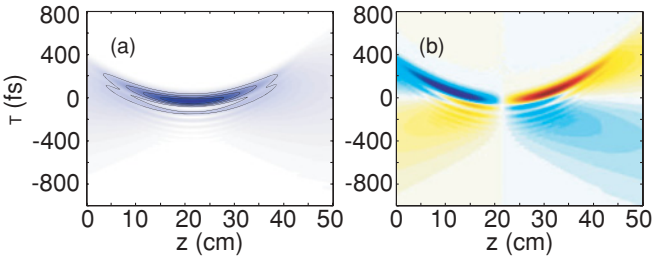

FIG. 8. (Color online) (a) Linear scale of the intensity plot and (b) longitudinal flux J_τ vs propagation distance z for a Gaussian pulse with strong quadratic and cubic frequency chirp. For both figures, the temporal axis refers to the local frame moving at $V_G = 1/k_0'$. The color scale of J_τ indicates flux toward positive (negative) τ values in red (blue).

longitudinal energy flux in itself, and second, we associate it with the transverse component to obtain the direction of the energy flux for general wave packets. To our knowledge, this was attempted only once with the Poynting vector associated with localized waves [41]. Here we consider the energy flux in the frame moving at the velocity of the envelope peak of specific WP to diagnose the energy redistribution occurring within the WP.

A. Longitudinal component of the energy flux

In the frame moving at $V_G = 1/k_0'$, the longitudinal flux component J_τ is related to the chromatic dispersion of the pulse, as indicated by Eq. (5). In both cases of normal and anomalous GVD, a Gaussian pulse with an initial flat phase develops during propagation a longitudinal flux component distinguished by two side lobes in the leading and in the trailing part of the pulse: the leading lobe is directed toward negative times and the trailing lobe toward positive times [Fig. 7(a)]. This indicates that the pulse is broadening along the temporal coordinate. In contrast, if the pulse has an initial negative chirp and propagates in a normally dispersive medium, each side lobe corresponds to a longitudinal flux with opposite sign, indicating pulse compression during propagation, as expected from the action of normal GVD.

The case of nonlinear propagation in a Kerr medium with anomalous dispersion is particularly instructive. Although we derived the energy flux from linear propagation equations in Sec. II, the expression for **J** also holds for nonlinear propagation and in the presence of losses, as we will illustrate in Sec. VI. Self phase modulation induced by the optical Kerr effect generates new frequencies in the regions of the pulse with the strongest intensity gradients. In particular, a focusing Kerr nonlinearity generates upshifted (downshifted) frequencies with respect to the central frequency in the decreasing (increasing) part of the pulse. In conjunction with with anomalous GVD, this effect is responsible for pulse shortening during propagation. Figure 7(b) illustrates the longitudinal flux obtained in this situation: Each lobe of J_τ exhibits an opposite sign with respect to the linear propagation case. Figure 7(c) depicts the longitudinal flux associated with the nonlinear propagation of a GP with lower energy and pulse intensity than that in Fig. 7(b). In this case, self phase modulation is weaker and the new frequencies are not able to overcome linear dispersion over the whole pulse. Nonlinear effects thus dominate in the central high-intensity core and the flux points inward, thus leading to a local temporal compression, while the surrounding low-intensity regions behave almost linearly with an outward flux. This leads to the progressive distortion of the pulse.

In analogy with the evolution of the temporally averaged transverse flux depicted in Figs. 2(a)–2(c), the evolution of the radially averaged longitudinal flux $\mathcal{J}_\tau$ may be regarded as the propagation of a pulse inside an optical fiber.

Figures 8(a) and 8(b) show the intensity and the longitudinal flux $\mathcal{J}_\tau$ versus propagation distance z for the linear propagation of a pulse with an initially Gaussian spectral distribution and strong quadratic and cubic phase chirp. The dispersion parameters correspond to propagation in water at a central wavelength of 527 nm. In this simulation we considered that only dispersive effects occur during propagation and neglected diffraction. The intensity pattern depicts an intense temporal peak whose velocity v varies during propagation, following the relation $1/v = 1/V_G + d\tau/dz$. In the local frame moving at V_G, the instantaneous velocity of this peak is given by the first derivative of the (τ, z) intensity distribution curve. The curvature of this intensity distribution thus represents the peak acceleration: in Fig. 8(a), the peak exhibits a constant deceleration. The peak velocity changes from superluminal for the first $\sim$20 cm to subluminal afterward. This behavior is governed by the cubic chirp, while the distance z at which the peak travels at V_G (i.e., the z position for which $d\tau/dz = 0$) is determined by the quadratic chirp. Note that a cubic chirp of opposite sign would lead to a constant acceleration, due to the change of the curvature sign. The longitudinal component of **J** shown in Fig. 8(b) illustrates the deceleration property: We observe in correspondence of the main peak a net flux directed toward negative (positive) times in the superluminal (subluminal) region. However, the overall pulse presents a broad series of secondary intensity peaks associated with a flux of opposite sign. This indicates, as expected, that the center of mass of the entire pulse energy does not change during propagation in spite of the peak deceleration. Furthermore, for large propagation distances [rightmost part of Fig. 8(b)], the flux pattern becomes similar to that obtained for a GP subject to normal GVD [see for example Fig. 7(a)].

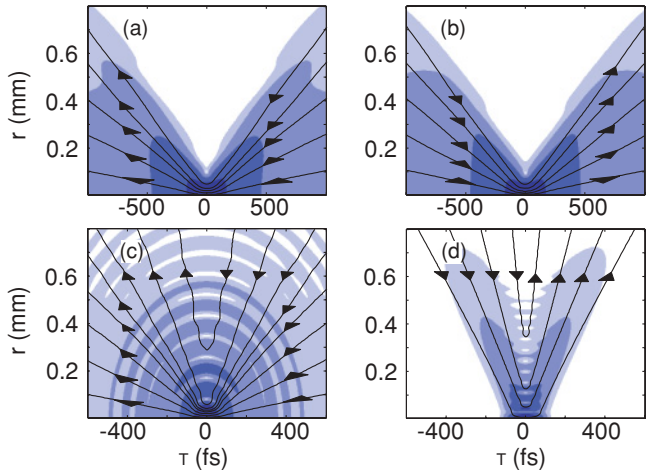

FIG. 9. (Color online) Streamline plot of vector **J** for stationary envelope wave packets. (a, b) subluminal and superluminal frequency-gap X waves, respectively, as in Fig. 5. (c) Subluminal O wave as in Fig. 6(a). (d) Superluminal wave-number-gap X wave with parameters like the ones of Fig. 5(b), but $T_p = 60$ fs and $\theta_0 = 0.005$ rad. The contour plots show the intensity over five decades.

B. Streamline representation of the flux

The longitudinal component is also useful for envisioning the direction of the energy density flux. In this context, the choice of the reference system is important; that is, the direction of the energy flux depends on the moving frame chosen to represent this quantity. For stationary-envelope WPs, a natural choice is the reference system moving at the peak velocity of the pulse, as expressed in Eqs. (17) and (18). Figure 9 illustrates four different cases of CWPs with stationary envelope. Figures 9(a), 9(b), and 9(c) show the streamline plots of vector **J** for the previously considered (Secs. IV A and IV B) subluminal and superluminal X waves with a frequency gap (as in regions $B^{\pm}$ of Fig. 1) and subluminal O wave (as in region D^{-} of Fig. 1), respectively. Figure 9(d) shows the energy-flux streamlines in the cases of a superluminal X wave with a wave number gap (region A of Fig. 1). The most important feature is that the energy flows along conical surfaces from the outer region toward the central peak and then streams outward again to the surrounding region. Moreover, along the temporal (longitudinal) coordinate, the flow is directed toward negative (positive) times for subluminal (superluminal) stationary conical wave packets. This result is in keeping with the fact that the peak results from a constructive interference supported by the surrounding energy reservoir: Even if the longitudinal velocity of the envelope peak V is superluminal (larger than V_G), the energy is actually transported along z at velocity $V_E = V_G \cos\theta_0$. As a last remark, it is worth noticing that the condition $\widetilde{\mathrm{div}}\mathbf{J} = 0$, which characterizes stationarity of the intensity profile of the envelope during its paraxial propagation along z, is satisfied by applying Eqs. (17) and (18) to any analytical solutions obtained by Malaguti and Trillo. This result is remarkable since these solutions are fully nonparaxial, whereas Eqs. (17) and (18) are obtained in a paraxial framework. This is actually due to the truncature of dispersive terms at second order for $k_\perp^2(\Omega)$ in the Malaguti and Trillo solutions.

We now give a geometrical interpretation of the the energy-flux streamlines in different regimes of GVD, highlighting uncovered links with the phase fronts.

By using a decomposition of the complex amplitude $\Psi \equiv |\Psi|\exp(i\phi)$ into a real amplitude and phase and by means of the local longitudinal coordinate transformation $\xi = -V_m\tau$, where $V_m \equiv (|\alpha_2|)^{-1/2}$, the components [Eqs. (17) and (18)] of the flux read

$$\mathbf{J}_\perp = \frac{1}{\beta}|\Psi|^2\nabla_\perp\phi(r,\xi,z) \tag{23}$$

$$J_\xi = -\frac{\mathrm{sgn}(\alpha_2)}{\beta}|\Psi|^2\left[\frac{\partial\phi}{\partial\xi}(r,\xi,z) + \frac{\mathrm{sgn}(\alpha_2)\alpha_1}{\sqrt{|\alpha_2|}}\right]. \tag{24}$$

The last term in Eq. (24) may be absorbed in the phase by using $\phi'(r,\xi,z) = \phi(r,\xi,z) + \frac{\mathrm{sgn}(\alpha_2)\alpha_1}{\sqrt{|\alpha_2|}}\xi$. The flux is then expressed as the product of the intensity $|\Psi|^2$ by vector $\mathbf{e}_J \equiv \beta^{-1}(\nabla_\perp\phi', -\mathrm{sgn}(\alpha_2)\partial\phi'/\partial\xi)$. Both the transverse and longitudinal components are then proportional to the phase gradient in the corresponding direction. Only in the case of an effective anomalous dispersion ($\alpha_2 < 0$) is the flux vector proportional to the phase gradient: $(\mathbf{J}_\perp, J_\xi) = \beta^{-1}|\Psi|^2\nabla\phi'(r,\xi,z)$, where ∇ denotes the gradient in the (x, y, ξ) space. In this case, the vector $(\mathbf{J}_\perp, J_\xi)$ is orthogonal to the isocontour for the phase $\phi'(r,\xi,z)$. This is shown, for example, in Fig. 10(d), where we plot $\mathbf{e}_J = \mathbf{J}/|\psi|^2$ as a vector field and the phase ϕ' as a color plot [50] for a GP centered at $\lambda_0 = 1300$ nm in water (anomalous GVD regime).

For $\alpha_2 > 0$, vector $\mathbf{e}_J$ represents the symmetric of the normal to the phase front with respect to the axis $\xi = 0$. This is a geometric property that follows from the definition of the flux. Consequently, the energy flux is such that phase fronts parallel to the loci $r = \pm\xi$ are associated with an energy flux parallel to the phase front. In the case of a GP, the possible regimes are represented in Figs. 10(a) and 10(b), where $\mathbf{e}_J$ is plotted over $\cos\phi'$ for different propagation distances z of the same GP having $z_R \neq z_{\mathrm{GVD}}$. Figure 10(a) refers to a short propagation distance ($z < z_R, z_{\mathrm{GVD}}$): the iso-$\phi'$ curves do not

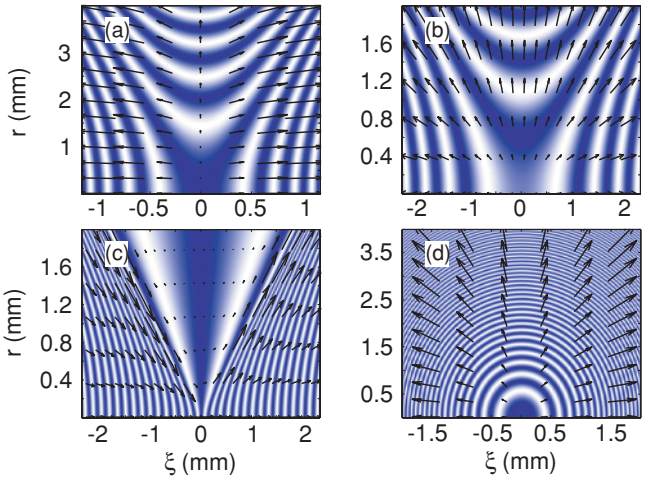

FIG. 10. (Color online) Vector $\mathbf{e}_J$ superimposed to the plot of $\cos\phi'$ for different cases. GP in normal GVD regime with $z_R \neq z_{\mathrm{GVD}}$ for short (a) and long (b) propagation distances. Note the differences in axis limits. (c) Subluminal frequency-gap X-wave profile. (d) GP in anomalous GVD regime.

follow $r = \pm\xi$ and $\mathbf{e}_J$ are neither orthogonal nor parallel to the phase fronts, but the symmetric vectors with respect to the axis $\xi = 0$ are clearly orthogonal to phase fronts. Figure 10(b) refers to a longer propagation distance ($z \gg z_R, z_{\mathrm{GVD}}$): since in this case the iso-phase curves asymptotically approach $r = \pm\xi$ [within a second-order approximation of $k(\omega)$], the vector field $\mathbf{e}_J$ and thus the flux $\mathbf{J}$ are asymptotically parallel to phase fronts along $r = \pm\xi$. This is also the case for the X wave with a frequency gap and an asymmetric spectral weight obtained from the analytical formula (24) of Ref. [8], as shown in Fig. 10(c) (subluminal case): the phase fronts align asymptotically along $r = \pm\xi$, even if in this region the intensity is very low, and thus $\mathbf{e}_J$ and the energy flux become asymptotically parallel to phase fronts.

This geometrical construction of flux streamlines from the phase fronts illustrates the link between the determination of the phase and that of the energy density flux for an optical WP propagating in a dispersive medium.

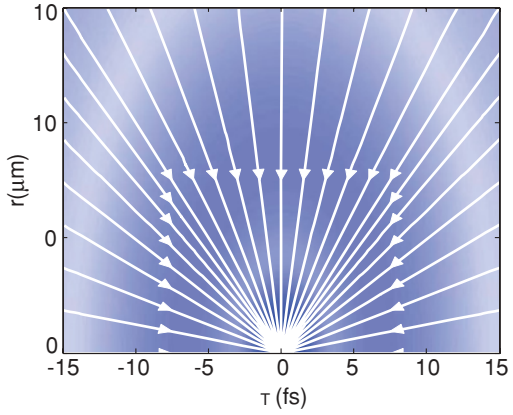

FIG. 11. (Color online) Streamline plot of the energy flux $\mathbf{J}$ for a nonlinear O wave (UBO) with stationary envelope propagating at $V_G = k_0'^{-1}$. The streamlines are superimposed to the intensity distribution of the UBO plotted over four decades.

VI. NONLINEARITY AND ABSORPTION

In the case of nonlinear propagation, expressions (3) and (5) of flux density determined in Sec. II remain valid. As an example, we consider the nonlinear propagation of conical wave packets such as those formed spontaneously during filamentation in water, which is described by the nonlinear envelope equation including nonlinear source terms for the optical Kerr effect with instantaneous and delayed (Raman effect) contributions, multiphoton absorption, and plasma effects (absorption and defocusing) following ionization of the medium [16,51]. In this case, Eq. (2) becomes

$$\frac{\partial|\mathcal{E}|^2}{\partial z} + \widetilde{\mathrm{div}}\mathbf{J} = -\beta^{(K)}|\mathcal{E}|^{2K} - \sigma\rho|\mathcal{E}|^2, \tag{25}$$

where the terms on the right-hand side of Eq. (25) represent the density of energy losses by multiphoton absorption and plasma absorption, respectively (see Ref. [25] for details). The parameters are the cross section $\beta^{(K)}$, where K denotes the number of photons involved in the multiphoton process, the cross section for inverse Bremsstrahlung σ, and ρ denotes the plasma density. Note that linear absorption can be treated similarly ($K \equiv 1$).

We therefore have an extension of the energy flux also in the nonlinear case and in the presence of absorption. In this case the continuity equation contains additional terms which represent the amount of energy transferred from the optical pulse to the medium.

Recently, nonlinear conical wave-packet profiles which maintain an intensity-invariant shape in the presence of nonlinear losses have been discovered [52,53]. Numerical solutions called unbalanced nonlinear Bessel beams (UBBs) and unbalanced nonlinear O waves (UBOs) have been found for the monochromatic case and the polychromatic case in the regime of anomalous GVD, respectively.

Following the procedure of Ref. [53], we numerically evaluated the near-field profiles of UBBs and UBOs and the associated energy flux.

Figure 11 shows the streamline representation of $\mathbf{J}$ for an UBO. The parameters were chosen to represent dispersion and nonlinear losses for water at $\lambda_0 = 1300$ nm. The energy flux is directed toward the center of the pulse corresponding to the peaks of intensity distribution and multiphoton absorption. The central core, that is, the intense part of the wave, is therefore continuously replenished by the conical nature of the pulse and this permits the stationary behavior in spite of losses. The energy flux carried by the conical tail actually exactly compensates the amount of losses in the intense core.

VII. DISCUSSION AND CONCLUSIONS

Since there is a close relation between the energy flux and the phase fronts, information on the energy flux constitutes a powerful tool for predicting if and how energy will be redistributed during propagation of the wave packet under examination. We have seen that knowledge of the magnetic field, which would be necessary to build the Poynting vector, is not necessary with the expressions for the energy flux derived in the present work. We emphasize here the approximations in which this study is valid.

First, it relies on a paraxial approximation. This may be overcome by means of an effective correction to the longitudinal component of the main wave vector, as in Eq. (16), which leads to similar types of expressions for the components of the energy flux [Eqs. (17) and (18)]. However, in experimental situations it is not always clear which angle should be considered as θ_0. In the paraxial case we may reduce to the assumption $\beta = k_0$.

Second, it is based on a second-order expansion of $k(\omega)$ around ω_0. It is possible to include higher-orders terms. Without going into the details, we give here the third-order correction to the longitudinal component of the energy flux:

$$J_\tau = \frac{ik_0''}{2}\left(\mathcal{E}^*\frac{\partial\mathcal{E}}{\partial\tau} - \mathcal{E}\frac{\partial\mathcal{E}^*}{\partial\tau}\right) + \frac{k_0'''}{6}\left(\mathcal{E}^*\frac{\partial^2\mathcal{E}}{\partial\tau^2} + \mathcal{E}\frac{\partial^2\mathcal{E}^*}{\partial\tau^2} - \frac{\partial\mathcal{E}^*}{\partial\tau}\frac{\partial\mathcal{E}}{\partial\tau}\right). \tag{26}$$

Other approximations are linked to the fact that we have neglected high-order operators in the propagation equation, such as the space-time focusing operator (which takes into account the fact that for each frequency there is a different

Rayleigh range) or self-steepening operator in the nonlinear case. These operators would give corrections to the flux expressions derived in this article, which can be obtained perturbatively as far as space-time coupling is concerned. The expressions obtained in the paraxial case represent a good approximation for wave packets with sufficiently narrow frequency bands; however, the corrections to the flux would be relevant for highly nonparaxial wave packets, single-cycle pulses or WPs with central frequency close to a zero in the GVD dispersion curve.

It has been shown that an envelope equation corrected with space-time focusing and self-steepening terms, that is, the nonlinear envelope equation, still properly describes the propagation of pulses at single-cycle durations [54]. The expression for the flux we have derived does not account for these terms and is therefore not expected to be accurate as we approach the single-cycle limit. A first possibility to make these expressions more accurate for few-cycle pulses is to derive corrections due to the additional space-time focusing term, in the linear case, by treating this term perturbatively as for the derivation of the nonlinear envelope equation. However, this procedure would yield expressions for the flux which are dependent on the choice of the carrier frequency and thus of k_0, whereas these quantities lose their significance for single-cycle pulses or large bandwidths. A second possibility would be to resort to unidirectional propagation equations such as those proposed by Kolesik and Moloney [55], which consider the propagation of the electric field for any pulse duration and would yield expressions for the flux that are independent of any reference frequency or wave number. The group velocity of the pulse, however, enters the propagation equation expressed in moving frame [56]. It is thus expected to enter the derived expression for the flux as well as the dispersive properties of the medium. Finally, an elegant possibility to obtain expressions for the flux that are independent of reference frequencies or wave number, valid for few-cycle pulses, and explicitly linked to the Poynting vector and electromagnetic energy density is indicated in Appendix B in the case of propagation in a nondispersive medium. A similar derivation for a dispersive medium goes beyond the scope of the present article but would be the easiest way to generalize the notion of energy density flux for few-cycle pulses and in particular to apply it to conical waves carrying a large spectrum.

In conclusion, we defined a concept of energy density flux which is slightly different from that of the Poynting vector since it mainly relies on the propagation equation for the complex amplitude of the wave packet and does not require knowledge of the magnetic field. The energy flux is intimately connected to the knowledge of amplitude and phase of the electric field in the local reference frame (x, y, τ) of the pulse under examination. In the case of pulses with strong spatiotemporal coupling, near-field measurements may be quite difficult to interpret [15]. The phase information, if available, is in general even less clear. We have shown that an analysis of optical pulses by means of the energy density flux $\mathbf{J}$ is a valuable tool for extracting and representing this phase information when dispersion of the medium can be truncated at second order. In particular, we have deeply analyzed the case of CWPs for stationary and nonstationary pulses and we have extended the procedure to the nonlinear case. The energy density flux was shown to be a useful tool for retrieving information about the nature of the pulse and its evolution during propagation. The most appealing feature of this tool is the possibility to adopt it in an experimental framework, as introduced in [32], thanks to the development of spatiotemporal intensity and phase retrieval techniques.

ACKNOWLEDGMENTS

Fruitful discussions with M. Cessenat are gratefully acknowledged.

APPENDIX A: LINK BETWEEN THE ENERGY DENSITY FLUX AND THE POYNTING VECTOR

We start by considering the electric field as mainly directed along the x axis and with zero y component ($|\mathbf{E}| \simeq E_x$). From Maxwell equations in the absence of free charges we have

$$\mathrm{div}\mathbf{D} = 0 \tag{A1}$$

and in the Fourier space (only temporal transformation), $\hat{\mathbf{D}}(\omega) = \epsilon_0 n^2(\omega)\hat{\mathbf{E}}(\omega)$. Equation (A1) may be written as

$$n^2 \frac{\partial \hat{E}_x}{\partial x} + \frac{\partial}{\partial z}(n^2 \hat{E}_z) = 0. \tag{A2}$$

It is possible now to treat this equation perturbatively, considering $\mathbf{E} = \boldsymbol{\mathcal{E}} \exp[ik_0 z - i\omega_0 t]$. We obtain, considering only the dominant terms,

$$\boldsymbol{\mathcal{E}} = \left\{ \mathcal{E}_x; 0; -\frac{1}{ik_0}\frac{\partial \mathcal{E}_x}{\partial x} \right\}. \tag{A3}$$

The magnetic field is obtained with a perturbative approach starting from the Maxwell equation:

$$\frac{\partial \mathbf{B}}{\partial t} = -\mathrm{rot}\mathbf{E}. \tag{A4}$$

By also considering $\mathbf{B} = \boldsymbol{\mathcal{B}} \exp[ik_0 z - i\omega_0 t]$, we obtain

$$\boldsymbol{\mathcal{B}} = \left\{ 0; \frac{k_0}{\omega_0}\mathcal{E}_x - i\frac{k_0}{\omega_0^2}\frac{\partial \mathcal{E}_x}{\partial t} - \frac{i}{\omega_0}\frac{\partial \mathcal{E}_x}{\partial z}; \frac{i}{\omega_0}\frac{\partial \mathcal{E}_x}{\partial y} \right\}. \tag{A5}$$

The Poynting vector in the case of a rapidly oscillating field is

$$\langle \mathbf{S} \rangle = \langle \mathbf{E} \times \mathbf{H} \rangle = \frac{1}{2\mu_0} \mathrm{Re}\left\{ \boldsymbol{\mathcal{E}} \times \boldsymbol{\mathcal{B}}^* \right\}. \tag{A6}$$

With the preceding expressions,

$$S_x = \frac{1}{2\mu_0} \mathrm{Re}\left\{ -\frac{i}{\omega_0} \mathcal{E}_x{}^* \frac{\partial \mathcal{E}_x}{\partial x} \right\}, \tag{A7}$$

$$S_y = \frac{1}{2\mu_0} \mathrm{Re}\left\{ +\frac{i}{\omega_0} \mathcal{E}_x \frac{\partial \mathcal{E}_x{}^*}{\partial y} \right\}, \tag{A8}$$

$$S_z = \frac{1}{2\mu_0} \mathrm{Re}\left\{ \frac{k_0}{\omega_0}|\mathcal{E}_x|^2 + \frac{ik_0}{\omega_0^2}\mathcal{E}_x \frac{\partial \mathcal{E}_x{}^*}{\partial t} + \frac{i}{\omega_0}\mathcal{E}_x \frac{\partial \mathcal{E}_x{}^*}{\partial z} \right\}. \tag{A9}$$

$\mathbf{S}$ is always given in $\mathrm{W/m^2}$. In the preceding equations the electric field is given in V/m. However, in deriving the evolution equation for the intensity from that for the envelope [Eq. (2)], we assumed that fields were in $(\mathrm{W/m^2})^{1/2}$. If we consider such a change of units in these equations, by

mean of a factor $\epsilon_0 c n_0$, the preceding equations become

$$S_x = \mathrm{Re}\left\{-\frac{i}{k_0}\mathcal{E}_x{}^*\frac{\partial \mathcal{E}_x}{\partial x}\right\}, \tag{A10}$$

$$S_y = \mathrm{Re}\left\{+\frac{i}{k_0}\mathcal{E}_x\frac{\partial \mathcal{E}_x{}^*}{\partial y}\right\}, \tag{A11}$$

$$S_z = \mathrm{Re}\left\{|\mathcal{E}_x|^2 + \frac{i}{\omega_0}\mathcal{E}_x\frac{\partial \mathcal{E}_x{}^*}{\partial t} + \frac{i}{k_0}\mathcal{E}_x\frac{\partial \mathcal{E}_x{}^*}{\partial z}\right\}. \tag{A12}$$

These equations show that the transverse components of the energy-flux vector $\mathbf{J}$, defined starting from the paraxial propagation equation, coincide with the transverse components of the Poynting vector $\mathbf{S}$. The longitudinal components are also related and the link is obtained by considering the continuity equation which produced the definition of $\mathbf{J}$, derived from the propagation equation, and the continuity equation of the Poynting vector. These two equations read as

$$\frac{\partial |\mathcal{E}|^2}{\partial z} = -\widetilde{\mathrm{div}}\mathbf{J} = -\boldsymbol{\nabla}_\perp \mathbf{J}_\perp - \frac{\partial J_t}{\partial t},$$

$$\frac{\partial}{\partial t}(w_e + w_m) = -\mathrm{div}\mathbf{S} = -\boldsymbol{\nabla}_\perp \mathbf{S}_\perp - \frac{\partial S_z}{\partial z},$$

where w_e and w_m represent electric and magnetic energy density, respectively. Since $\mathbf{J}_\perp = \mathbf{S}_\perp$ within the approximations involved, we thus identify

$$\frac{\partial J_t}{\partial t} = \frac{\partial}{\partial z}(S_z - |\mathcal{E}_x|^2) + \frac{\partial}{\partial t}(w_e + w_m). \tag{A13}$$

APPENDIX B: ENERGY FLUX WITHOUT ENVELOPE APPROXIMATION

We have emphasized that the validity range of the expressions for the energy density flux derived in this work mainly arise from the envelope approximation. We indicate here a possible route to generalize the expressions for the energy density flux to the case of few-cycle pulses propagating in a *nondispersive medium*. We link the generalized flux with the Poynting vector.

A. Potential function

Green and Wolf have shown that any electromagnetic field may be rigorously derived from a single, generally complex, scalar wave function $V(\mathbf{r}, t)$ [33]. Under the gauge condition $\boldsymbol{\nabla} \cdot \mathbf{A} = 0$, where $\mathbf{A}$ denotes the usual vector potential. The real and imaginary parts of the scalar complex function V simply represent the two components of $\mathbf{A}$ that are orthogonal to the wave vector. The function V allows a simple derivation of the momentum density $\mathbf{g}(\mathbf{r}, t)$ and the energy density $w(\mathbf{r}, t)$ of the field. In a homogeneous isotropic medium, these quantities were shown to be represented by expressions analogous to the formulas for the probability current and the probability density in quantum mechanics:

$$w = \frac{\epsilon_0}{2}\left[\boldsymbol{\nabla} V \cdot \boldsymbol{\nabla} V^* + \frac{1}{c^2}\frac{\partial V}{\partial t}\frac{\partial V^*}{\partial t}\right], \tag{B1}$$

$$\mathbf{S} = c\mathbf{g} = -\frac{\epsilon_0}{2}\left[\frac{\partial V^*}{\partial t}\boldsymbol{\nabla} V + \frac{\partial V}{\partial t}\boldsymbol{\nabla} V^*\right]. \tag{B2}$$

These quantities satisfy the usual conservation law,

$$\frac{\partial w}{\partial t} = -\boldsymbol{\nabla} \cdot \mathbf{S}, \tag{B3}$$

and $\mathbf{S}$ is the standard Poynting vector.

B. Generalized flux for single-cycle pulses

Equation (B3) can be rewritten in a form similar to that obtained from a unidirectional propagation equation where the evolution variable is z and time t plays the role of a longitudinal coordinate:

$$\frac{\partial S_z}{\partial z} + \frac{\partial w}{\partial t} = -\boldsymbol{\nabla}_\perp \cdot \mathbf{S}_\perp. \tag{B4}$$

By a change of reference frame $\xi = z$, $\tau = t - z/c$, the derivatives are transformed as $\partial/\partial t = \partial/\partial\tau$ and $\partial/\partial z = \partial/\partial\xi - (1/c)\partial/\partial\tau$. Equation (B4) becomes

$$\frac{\partial S_z}{\partial \xi} = -\boldsymbol{\nabla}_\perp \cdot \mathbf{S}_\perp - \frac{\partial}{\partial \tau}(w - S_z/c). \tag{B5}$$

This is the generalization of the energy-conservation equation, without envelope approximation, which also establishes the link with the usual Poynting vector. The left-hand side describes the evolution of the longitudinal component of the Poynting vector S_z with respect to the evolution variable ξ; it may be regarded as the energy density in the (x, y, τ) space since it represents the intensity of the optical field. The right-hand side is the divergence $(\widetilde{\boldsymbol{\nabla}} \cdot \mathbf{v} = \boldsymbol{\nabla}_\perp \cdot \mathbf{v}_\perp + \partial v_\tau/\partial\tau)$ of the flux vector with components $(\mathbf{S}_\perp, w - S_z/c)$ in the perpendicular and longitudinal τ directions, respectively. The longitudinal flux component is proportional to the difference between the usual density of electromagnetic energy w and the longitudinal component of the Poynting vector. The transverse component of the flux is the same as that of the Poynting vector $S_\perp$, whether the envelope approximation is made or not. The flux components do not depend on the choice of a carrier frequency or wave number. These expressions were obtained in a medium without dispersion and would require to be further generalized in dispersive media. Although this full generalization is beyond the scope of the article, one can note that Eq. (B5) is similar to Eq. (2), which was derived in a dispersive medium under the envelope approximation. The generalized flux is expected to depend on the dispersive properties of the medium since the electromagnetic energy w depends on the dielectric permittivity. We finally note that the fact that S_z and $w - S_z/c$ can be interpreted as an energy density in the (x, y, τ) space and a longitudinal flux component, respectively, is not obvious; thus, we show in the next section that these expressions allow us to retrieve the flux expressions obtained under the envelope approximation.

C. Link with the envelope formulation

In order to show the connection with the envelope formulation, we assume that the field, and hence the potential V, can be expressed as $V = U\exp[i(\phi - \omega_0 t + k_0 z)]$, where ω_0 and k_0 are the frequency and wave number of the carrier wave, U is a real envelope, and ϕ the phase of the potential V. The

energy density and energy-flux components then read

$$S_z = -\frac{\epsilon_0}{2}\left(\frac{\partial V^*}{\partial t}\frac{\partial V}{\partial z} + \frac{\partial V}{\partial t}\frac{\partial V^*}{\partial z}\right)$$
$$= \epsilon_0\left\{U^2\left[\omega_0 k_0 - \frac{\partial\phi}{\partial t}\frac{\partial\phi}{\partial z} - k_0\frac{\partial\phi}{\partial t} + \omega_0\frac{\partial\phi}{\partial z}\right] - \frac{\partial U}{\partial t}\frac{\partial U}{\partial z}\right\}, \quad \text{(B6)}$$

$$\mathbf{S}_\perp = -\frac{\epsilon_0}{2}\left(\frac{\partial V^*}{\partial t}\boldsymbol{\nabla}_\perp V + \frac{\partial V}{\partial t}\boldsymbol{\nabla}_\perp V^*\right)$$
$$= \epsilon_0\left[U^2\left(\omega_0 - \frac{\partial\phi}{\partial t}\right)\boldsymbol{\nabla}_\perp\phi - \frac{\partial U}{\partial t}\boldsymbol{\nabla}_\perp U\right], \quad \text{(B7)}$$

$$w - S_z/c = \frac{\epsilon_0}{2}\left[\boldsymbol{\nabla}_\perp V\cdot\boldsymbol{\nabla}_\perp V^* + \frac{\partial V}{\partial\xi}\frac{\partial V^*}{\partial\xi}\right]$$
$$= \frac{\epsilon_0}{2}\left\{(\boldsymbol{\nabla}_\perp U)^2 + \left(\frac{\partial U}{\partial\xi}\right)^2 + U^2\left[(\boldsymbol{\nabla}_\perp\phi)^2 + \left(\frac{\partial\phi}{\partial\xi}\right)^2\right]\right\}. \quad \text{(B8)}$$

The preceding equations are still exact. (No envelope approximation was made.) In the envelope approximation, some terms in the preceding equations can be neglected. For example, $(\partial_t U)(\partial_z U) \ll \omega_0 k_0 U^2$. The energy density and flux then read

$$S_z \sim \epsilon_0\omega_0 k_0 U^2, \quad \text{(B9)}$$

$$\mathbf{S}_\perp \sim \epsilon_0\omega_0 U^2(\boldsymbol{\nabla}_\perp\phi), \quad \text{(B10)}$$

$$\frac{\partial}{\partial\tau}(w - g_z) \ll \boldsymbol{\nabla}_\perp\cdot S_\perp. \quad \text{(B11)}$$

By introducing these expressions in Eq. (B5), we obtain

$$k_0\frac{\partial}{\partial\xi}U^2 = -\boldsymbol{\nabla}_\perp\cdot[U^2(\boldsymbol{\nabla}_\perp\phi)]. \quad \text{(B12)}$$

Since $\mathbf{E} = -\partial\mathbf{A}/\partial t$, in the envelope approximation, $\mathcal{E} = i\omega_0\mathcal{A}$. The complex potential V just contains the components of the vector potential $\mathbf{A}$; hence, U is proportional to $\mathcal{E}$. The conservation equation [Eq. (B12)] then becomes similar to Eqs. (2) and (6) in the limit of a nondispersive medium. The expressions we have obtained (and the associated geometrical properties) are therefore valid in the limit of the envelope approximation.

[1] H. Nishioka, W. Odajima, K. Ueda, and H. Takuma, Opt. Lett. **20**, 2505 (1995).
[2] C. DAmico, A. Houard, S. Akturk, Y. Liu, J. Le Bloas, M. Franco, B. Prade, A. Couairon, V. T. Tikhonchuk, and A. Mysyrowicz, New J. Phys. **10**, 013015 (2008).
[3] M. Tabak, J. Hammer, M. E. Glinsky, W. L. Kruer, S. C. Wilks, J. Woodworth, E. M. Campbell, M. D. Perry, and R. J. Mason, Phys. Plasmas **1**, 1626 (1994).
[4] C. L. Arnold, A. Heisterkamp, W. Ertmer, and H. Lubatschowski, Appl. Phys. B **80**, 247 (2005).
[5] A. Vogel, J. Noack, G. Hüttman, and G. Paltauf, Appl. Phys. B **81**, 1015 (2005).
[6] V. Garces-Chavez, D. McGloin, H. Melville, W. Sibbett, and K. Dholakia, Nature (London) **419**, 145 (2002).
[7] V. Garces-Chavez, D. Roskey, M. D. Summers, H. Melville, D. McGloin, E. M. Wright, and K. Dholakia, Appl. Phys. Lett. **85**, 4001 (2004).
[8] S. Malaguti and S. Trillo, Phys. Rev. A **79**, 063803 (2009).
[9] J. Durnin, J. J. Miceli, and J. H. Eberly, Phys. Rev. Lett. **58**, 1499 (1987).
[10] J. Lu and J. F. Greenleaf, IEEE Trans. Ultrason. Ferroelectr. Freq. Control **37**, 438 (1990).
[11] P. Saari and K. Reivelt, Phys. Rev. Lett. **79**, 4135 (1997).
[12] Z. Liu and D. Fan, J. Mod. Opt. **45**, 17 (1998).
[13] P. Di Trapani, G. Valiulis, A. Piskarskas, O. Jedrkiewicz, J. Trull, C. Conti, and S. Trillo, Phys. Rev. Lett. **91**, 093904 (2003).
[14] M. Kolesik, E. M. Wright, and J. V. Moloney, Phys. Rev. Lett. **92**, 253901 (2004).
[15] D. Faccio, A. Matijosius, A. Dubietis, R. Piskarskas, A. Varanavicius, E. Gaizauskas, A. Piskarskas, A. Couairon, and P. Di Trapani, Phys. Rev. E **72**, 037601 (2005).
[16] A. Couairon, E. Gaizauskas, D. Faccio, A. Dubietis, and P. Di Trapani, Phys. Rev. E **73**, 016608 (2006).
[17] D. Faccio, P. Di Trapani, S. Minardi, A. Bramati, F. Bragheri, C. Liberale, V. Degiorgio, A. Dubietis, and A. Matijosius, J. Opt. Soc. Am. B **22**, 862 (2005).
[18] D. Faccio, A. Averchi, A. Dubietis, P. Polesana, A. Piskarskas, P. Di Trapani, and A. Couairon, Opt. Lett. **32**, 184 (2007).
[19] D. Faccio, M. A. Porras, A. Dubietis, G. Tamošauskas, E. Kučinskas, A. Couairon, and P. Di Trapani, Opt. Commun. **265**, 672 (2006).
[20] D. Faccio, A. Averchi, A. Couairon, M. Kolesik, J. V. Moloney, A. Dubietis, G. Tamosauskas, P. Polesana, A. Piskarskas, and P. Di Trapani, Opt. Express **15**, 13077 (2007).
[21] J. Trull, O. Jedrkiewicz, P. Di Trapani, A. Matijosius, A. Varanavicius, G. Valiulis, R. Danielius, E. Kucinskas, A. Piskarskas, and S. Trillo, Phys. Rev. E **69**, 026607 (2004).
[22] P. Gabolde and R. Trebino, Opt. Express **12**, 4423 (2004).
[23] C. Dorrer, E. M. Kosik, and I. A. Walmsley, Opt. Lett. **27**, 548 (2002).
[24] F. Bragheri, D. Faccio, F. Bonaretti, A. Lotti, M. Clerici, O. Jedrkiewicz, C. Liberale, S. Henin, L. Tartara, V. Degiorgio, P. Di Trapani, Opt. Lett. **33**, 2952 (2008).
[25] P. Polesana, M. Franco, A. Couairon, D. Faccio, and P. Di Trapani, Phys. Rev. A **77**, 043814 (2008).
[26] D. Faccio, A. Averchi, A. Lotti, P. Di Trapani, A. Couairon, D. Papazoglou, and S. Tzortzakis, Opt. Express **16**, 1565 (2008).
[27] F. Courvoisier, V. Boutou, J. Kasparian, E. Salmon, G. Méjean, J. Yu, and J.-P. Wolf, Appl. Phys. Lett. **83**, 213 (2003).
[28] M. Mlejnek, M. Kolesik, J. V. Moloney, and E. M. Wright, Phys. Rev. Lett. **83**, 2938 (1999).
[29] W. Liu, F. Théberge, E. Arévalo, J.-F. Gravel, A. Becker, and S. L. Chin, Opt. Lett. **30**, 2602 (2005).
[30] A. Dubietis, E. Gaižauskas, G. Tamošauskas, and P. Di Trapani, Phys. Rev. Lett. **92**, 253903 (2004).

[31] A. Dubietis, E. Kučinskas, G. Tamošauskas, E. Gaižauskas, M. A. Porras, and P. Di Trapani, Opt. Lett. **29**, 2893 (2004).
[32] D. Faccio, A. Lotti, A. Matijosius, F. Bragheri, V. Degiorgio, A. Couairon, and P. Di Trapani, Opt. Express **17**, 8193 (2009).
[33] H. S. Green and E. Wolf, Proc. Phys. Soc. A **66**, 1129 (1953).
[34] E. Wolf, Proc. Phys. Soc. **74**, 269 (1959).
[35] P. Roman, Proc. Phys. Soc. **74**, 281 (1959).
[36] L. Allen, M. J. Padgett, and M. Babiker, Prog. Opt. **39**, 291 (1999).
[37] F. Bonaretti, D. Faccio, M. Clerici, J. Biegert, and P. Di Trapani, Opt. Express **17**, 9804 (2009).
[38] P. Bowlan, P. Gabolde, A. Shreenath, K. McGresham, R. Trebino, and S. Akturk, Opt. Express **14**, 11892 (2006).
[39] P. Bowlan, U. Fuchs, R. Trebino, and U. D. Zeitner, Opt. Express **16**, 13663 (2008).
[40] H. I. Sztul and R. R. Alfano, Opt. Express **16**, 9411 (2008).
[41] E. Recami, Physica A **252**, 586 (1998).
[42] M. A. Porras, G. Valiulis, and P. Di Trapani, Phys. Rev. E **68**, 016613 (2003).
[43] P. Bowlan, H. Valtna-Lukner, M. Lõhmus, P. Piksarv, P. Saari, and R. Trebino, Opt. Lett. **34**, 2276 (2009).
[44] M. A. Porras and P. Di Trapani, Phys. Rev. E **69**, 066606 (2004).
[45] S. Orlov and A. Stabinis, Opt. Commun. **240**, 1 (2004).
[46] S. Longhi, Opt. Lett. **29**, 147 (2004).
[47] A. C. Newell and J. V. Moloney, *Nonlinear Optics* (Addison-Wesley, Redwood City, CA, 1992).
[48] A. G. Van Engen, S. A. Diddams, and T. S. Clement, Appl. Opt. **37**, 5679 (1998).
[49] S. Malaguti, G. Bellanca, and S. Trillo, Opt. Lett. **33**, 1117 (2008).
[50] Note that in Figs. 10(a)–10(d) we plot $\cos\phi'$ rather than ϕ' in order to render the phase profile more readable without unwrapping it. Isocontours for ϕ' are also isocontours for $\cos\phi'$ and the previously mentioned orthogonality property thus still holds with a representation of $\cos\phi'$.
[51] A. Dubietis, A. Couairon, E. Kučinskas, G. Tamošauskas, E. Gaižauskas, D. Faccio, and P. Di Trapani, Appl. Phys. B **84**, 439 (2006).
[52] M. A. Porras, A. Parola, D. Faccio, A. Dubietis, and P. Di Trapani, Phys. Rev. Lett. **93**, 153902 (2004).
[53] M. A. Porras, A. Parola, and P. Di Trapani, J. Opt. Soc. Am. B **22**, 1406 (2005).
[54] T. Brabec and F. Krausz, Phys. Rev. Lett. **78**, 3282 (1997).
[55] M. Kolesik and J. V. Moloney, Phys. Rev. E **70**, 036604 (2004).
[56] M. B. Gaarde and A. Couairon, Phys. Rev. Lett. **103**, 043901 (2009).